RSC Advances

ROYAL SOCIETY OF CHEMISTRY

www.rsc.org/advances

RCS Advances

RSCPublishing

ARTICLE

Demonstrating microdroplet coalescence for tailored and biodegradable microgel fabrication

Cite this: DOI: 10.1039/x0xx00000x

G. Simone[a]*

Received ooth January 2012,
Accepted ooth January 2012

DOI: 10.1039/x0xx00000x

www.rsc.org/

Coalescence of droplets is a microscopic phenomenon that is frequently occurring in Nature. Microfluidics can mimic those phenomena. In this field, the coalescence of microdroplets is widely in use for several processes such as synthesis of organic or inorganic nano- or micro-particles, mixing or design of biological or chemical components for medical applications. Here, a microfluidic design for passive coalescence of microdroplets has been analysed demonstrating a simplified mechanism for fusing the droplets (without synchronisation and phase of the droplets). An intriguing application of this "lab-on-a-chip" has been the formation of high aspect ratio biodegradable microgels via stabilisation with crosslinker (aldehydes). Geometrical aspect ratio, absorption, and biodegradability can be tuned by controlling the mode of coalescence. Those protein microgels and their derivatives can be considered as "smart materials" and may be applied in the biological or medical field. Microgel biodegradability which indicates good biocompatibility for those materials has been also investigated displaying characteristic time ranging from 1hrs to 5hrs.

1. Introduction

Coalescence is a common phenomenon in both Nature and technology and it plays an important role in many microscopic processes such as rain drop formation and coagulation of emulsions.[1-2] It is characterised by an initial formation of a liquid neck as two droplet surfaces touch. The neck radius affects the Laplace pressure that converges when the curvature of the liquid boundary is infinite, i.e. as the drops first touch.[3-4] Moreover, the underlying mechanism of coalescence can be inertia- as well as viscosity- driven.[5-6] In the very beginning of coalescence, the mechanism is limited by inertia caused by an instantaneous increase of the velocity of the two fusing droplets. During the last phases of coalescence, the viscous regime, in which the viscosity of the liquid limits the motion of the droplets, is the dominant mechanism. Indeed, in polymer solutions a viscous regime is the first step of coalescence. Viscous and inertial coalescence and transition are defined by the Reynolds number of the coalescence.[7-8]

Droplet coalescence has been widely analysed. It grasped the attention of theoretical scientists as well as of experimental researchers.

The formation of microdroplets via coalescence is extensively used in microfluidics.[1, 9-11] The main applications include monitoring chemical reactions, biological assays and micro- or nanoparticle synthesis.[12-14] The coalescence of droplets (performed in free environment or in microfluidics) becomes more difficult for high viscous fluids.

Moreover, coalescence can be either passive or active depending on its origin. Passive coalescence is initiated by features of the microfluidic chip design such as channel width and channel necks. Active coalescence can be promoted by applying external forces.[15] Here we propose a method to perform passive coalescence by microfluidic design. We used T-junctions to generate droplets and a "shuffling element" (or "coalescence element") to fuse droplets. The microfluidic design leads to microdroplet coalescence, avoiding synchronisation of each phase of two different droplets.

The microfluidic system was characterised by experimental and numerical investigations. The fluid-dynamic investigation based on various Reynolds numbers of the fluid flow inside the microchannel confirmed the possibility to achieve viscous and inertial coalescence by varying the properties of the perfused streams. In turn these results were confirmed by the numerical analysis.

In order to demonstrate the validity of our method, protein microparticles with a high aspect ratio were made. The particles were composed of gelatin which was stabilised in the microfluidic channel. At room temperature, the gelatin is a solid gel, while increasing the temperature; it becomes a high viscous liquid requiring an adequate design to be handled. To date, the microfluidic channel has been *ad hoc* designed for the application.

The formation of the particles can be tailored to form high aspect ratio microgels. Furthermore, protein microgels can be considered as "smart materials" since their properties can be easily altered via crosslinking or surface functionalisation with bioactive components such as antigens or antibodies. Running the experiments, many interesting results related to the physics of the coalescence have been found. The understanding of the physics of the coalescence of gelatin and aqueous solutions could be of wide interest to control the design and the properties of the particles.

For such and other applications biodegradability is of crucial importance and was investigated in this study.

2. Experimental

2.1. Materials

The water used in all experiments was prepared in three–stage Millipore Milli-Q purification (resistivity of the system 18.2 M). Fluorinated oil was purchased from Solvay Plastics. For the high viscous experiments and for the proof of concept experiment a protein solution (gelatin, dynamic viscosity: 10.0 mPa s) was obtained from Sigma Aldrich (Italy) and used without further purification. The protein was prepared as a 15 wt% solution and kept at 35°C.

2.2. Microfluidic device

The experiments were carried out in a microfluidic chip made of a Polydimethylsiloxane (PDMS) – glass composite. The mould for PDMS was fabricated in Plexiglas by using micromilling (Minitech CNC Mini-Mill, US) and a tip with diameter 100 μm (Performance Micro-Tool, US). Subsequently, replica of the mould was made by mixing PDMS and fluorosilane which was then poured into the mould (**see Fig. 1S in Supporting Information**). After polymerisation at 90ºC for 2 h, the PDMS replica and glass slide (Dow Corning, Italy 50×75 mm) were sealed by surface plasma radicalisation of the two surfaces. In order to reduce wettability, the microfluidic channel was functionalised with fluorosilane (Fluorolink®). [16-18] The depth of the channel was 100 μm. The microfluidic chip had three inlets (A, B and C). At the distance of 4 cm from the inlet A, the main channel widened and connected to a fluidic element labelled ”shuffling element” or “coalescence element”. The latter was connected to the inlet B. At the exit of the shuffling element, the channel width was 140 μm and the restriction after the shuffling element was 100 μm wide. The flow rate was controlled by a syringe pump (Nemesys apparatus). Glass syringes (1mL and 2.5 mL) and EPFT tubes (0.8 mm ID) were used.

2.3. Analysis of the droplets

Droplets flowing in the channel were observed using an inverted microscope (Olympus Flash IX-71) with a 4 and 10× objective lens in order to cover the whole area where droplet formation occurred. Image sequences were collected with a fast camera (CCD Hamamatsu Orca 3.6) at a frame rate variable between 10 and 600 fps depending on the flow rate. The observations were all made at a fixed distances and positions, in particular at (1) the orifices of droplet formation and (2) L=2 cm from the trap. In the high viscosity experiment, the temperature was kept at 40ºC. The protocols and the setup used for the experiment were described in our previous publication. [19] Furthermore, some experiments were carried out in order to stabilise microgel particles with cross-linkers. For the high viscosity experiments and the proof-of-concept experiments gelatin and different aldehydes were used. The aldehyde crosslinkers (i.e. formaldehyde and glutaraldehyde) were purchased from Sigma-Aldrich and used in concentration ranging from 0.1% to 10% . For flow analysis and in order to investigate the role of the flow rate at the inlet B, the frequency of droplet A and B was investigated. The frequency was achieved by analysing the movies recorded during the experiment by software Image J. After the analysis, the variation of signal intensity versus time was plotted (the z-stack of the regions of interest (ROIs) selected).

3. Results and discussion

3.1. Droplet generation

Fig.1a shows the microfluidic channel whilst the inset below displays the shuffling element (also **see Fig.1SSupporting Information**). The letters A to C, C′ refers to the inlets and the corresponding channels; J1 refers to the shuffling element. To indicate which flow rate was in which channel we used those letters as subscripted characters of the flow rate (Q_i).

An electric circuit analogue, shown in Fig.1b, assisted the device design. Indeed, each microchannel offered a certain resistance R to the flow($R \approx 12\mu L/hw^3$, where L was the length of a channel and h was the smaller of the two dimensions (h × w) of its rectangular cross-section and corresponded to the channel high and μ is the viscosity of the fluid).

In general, the most important prerequisite for efficient performance as a microdroplet generator is the flow stability, in particular at the drop formation node (in Fig. 1b the formation node in label as 1).

Given the length and the width of the microchannels, the flow rates can be identified as the governing parameter of microfluidics. This approach suggests that several applications for the microfluidic device can be envisaged easily just *tuning the individual flow rates*.

The microfluidic system shown in Fig.1 includes three inlets (A, B and C).

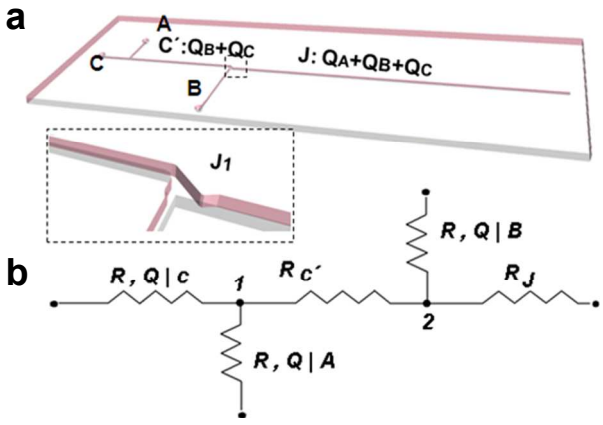

Fig.1. a) Isometric view of the microfluidic device. b) Electric circuit analogue.

By applying Kirchhoff principle at the two nodes where the droplets were formed (in Fig. 1b the node 1 and 2), the following equations were derived:

Node 1: $Q_C + Q_A = Q'_C$ (1)
Node 2: $Q_J = Q_B + Q'_C$ (2)

Combining the two equations, the flow rate at the B inlet was:
$\boldsymbol{Q_B} = Q_J - Q_C - Q_A$ (3)

According to Eq. (3), in order to generate the droplets, the flow rate in B was not independent variable but it was a function of the flow rates A and C (Q_C and Q_A). The flow rate in B is referred as Q_B. However, for convenience, the flow rate in B that is given by Eq. (3) is referred as Q_B*,(Q_B=Q_B*), while Q_B is the generic flow rate of B.

As a first analysis, we studied the dynamics of droplet formation at Q_B=Q_B* (Fig.2a). The images captured during the formation of water-in-oil-droplets displayed that both A and B droplets were formed. Analysing the frequency of the drop formation, it was observed that the two recorded frequencies overlapped(Fig. 2b). Once formed, A and B droplets flowed close to each other.

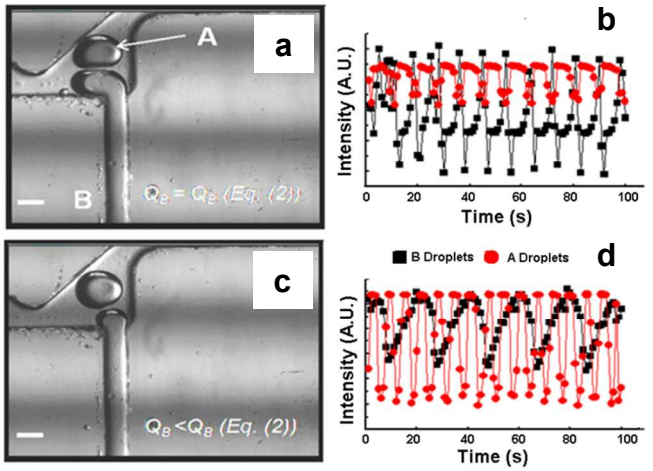

Fig.2. Analysis of droplet formation according to the flow rates of the droplet B. a) Images at the fluidic trap at Q_B=Q_B*. b) Frequency of droplet A and B formation at Q_B=Q_B*. c) Images at the fluidic trap at QB<QB*. d) Frequency of droplet A and B formation at Q_B<Q_B*. Bar scale: 100 μm.

By decreasing the flow rate of B, in order to have Q_B<Q_B* (Fig.2c),it was observed that, at the time the droplet A crossed the shuffling element, the droplet B was not yet formed.

Under this condition, the flow rate of the droplet A prevented the formation of the droplet B. At Q_B<Q_B*, the number of droplet B per droplet A crossing the fluidic coalescence element was lower than 1, the ratio A-to-B was 4:1 (Fig.2d). In conclusion, at Q_B<Q_B*, 1 droplet A out of 5 had a chance to coalesce with one droplet B. All experiments described above were carried out at the following flow rates, Q_A=1 μl/min, Q_B(<Q_B*)= 0.20 μl/min, Q_B(=Q_B*)= 0.50 μl/min. Furthermore, investigations using the microfluidic device indicate that droplet length depended on the flow rate (see **Fig. 2Sa and Fig. 2Sb Supporting Information**).

3.2. Droplet coalescence

Once the droplets were generated, the coalescence could take place. In order to extend the field of application of the microfluidic device, it is important to understand the behaviour of the droplets formed from streams having different chemical-physics behaviour.

Aqueous droplets have extensive value for the investigations involving cells, assays and handling of biological solutions.

Fig. 3 summarises the experimental and numerical findings of coalescence. First, the microfluidic coalescence element was tested with the system water-oil-water (A-C-B inlets) at the condition Q_B=Q_B* (to guarantee the formation of the droplets). The panels a and b in Fig. 3 show two timeframes extracted by the movies recorded during the experiments. The first timeframe displayed the flow of droplet A and droplet B, confirming the formation of the droplets at the analysed conditions (Fig. 3a). At the exit of the fluidic trap, the droplets flowed close to each other. Then, they first touched forming a liquid neck (condition that physically corresponds to the divergence of the Laplace pressure). At the time of image recording, the liquid neck had a curvature radius R=39 μm (Fig.3b). The shuffling element slowed down the droplet A and contributed to coalescence mechanisms permitting the droplets to travel close to each other and reach the critical distance.

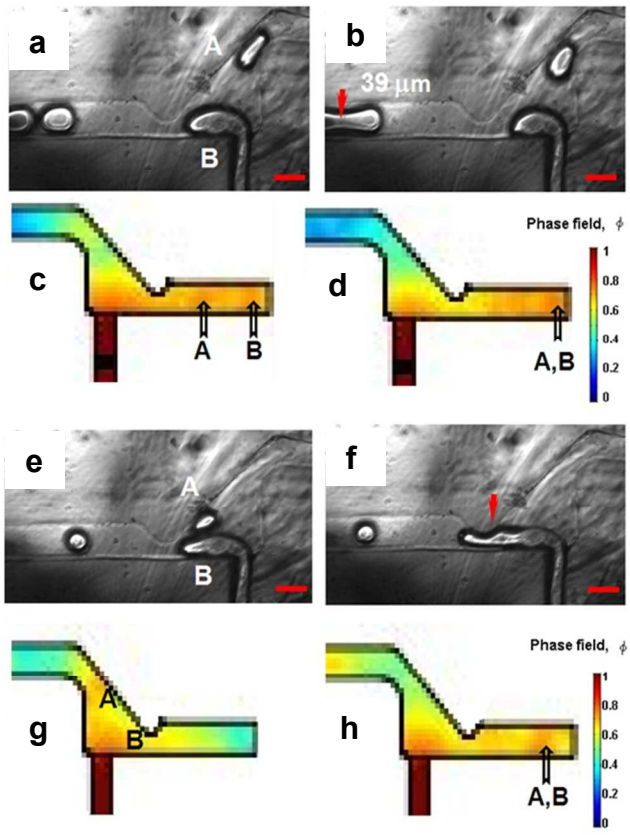

Fig.3 .Mechanisms of coalescence: experimental and numerical results. Q_B=Q_B*- Water Droplets. Experimental: a) A and B droplets travelled along the channel and b) formed a liquid bridge with a radius R (R=39 μm). Numerical: c) coalescence and d) fusion of the two nucleuses. Q_B=Q_B*- Viscous protein solution - Experimental: e) A and B droplets were formed and enter the fluidic trap. f) The coalescence occurs inside the channel. Numerical: g) A and B droplets travel together and fuse, h) and travel inside the channel. Bar Scale: 200 μm. Bar Scale (at the bottom of the panel) ranges from 0 to 1 and in particular, 0<φ<1. φ=0 for oil, φ=1 the pure A and B. The geometrical model and the pictures are displayed in opposite direction.

To model the mechanisms occurring inside the microfluidic channel, the fluidic phenomena of droplet formation and coalescence could be schematised by the momentum and continuity equations and the two phase-flow. [20-21]
Here, a model has been implemented by COMSOL software using the two phase-flow module. This module gives the possibility to control the intrinsic properties of the fluids. The laminar inflow at the inlets, with defined volume flows, was the initial condition. At the outflow boundary, no viscous stress condition was applied (**see Fig.3S Supporting Information** for the boundary conditions).

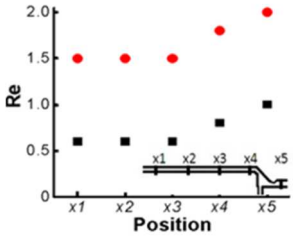

Fig.4. Reynolds number according to the position inside the channel. Re>1 for the condition Water and was Re<1 for the protein solution.

The results of the numerical model, based on the aqueous solution, are shown in panel c and d of Fig. 3. The droplets (see arrows that highlighted them) flowed inside the channel and inside the shuffling element. Then, their surfaces touched, but two cores (orange nucleus) were still distinguished as separate entities.
The mechanism of fusion of water-in-oil-droplets, as described by model, and confirmed by the investigation, included three steps: 1. the droplets formation, 2. droplets travelled close each other, 3.the droplets fused and the two cores merged.
This last step is reported in Fig.3d and displayed the droplets fused forming a unique core.

In order to extend the range of applications of the microfluidic device, the role of viscosity on the behaviour of the system was investigated.
Instead of water, a viscous solution was perfused at the inlet A.
The first consequence of the increased viscosity of the stream concerned the Capillary number ($Ca=\mu v/\gamma$). The Capillary number is function of the viscosity and surface tension (γ), however, while using the proteins, the viscosity of the stream changes, the surface tension remain unaltered (the surface tension of the viscous solution (protein) was 0.0046 N/m and the surface tension of water 0.003 N/m). [22]
The increased viscosity, μ, affects the resistance of the channel, to date, in respect to the experiment run with water, different flow rates were required.

The set of experiments were carried out at the following flow rates: Q_A=1µl/min, Q_B(=Q_B*)=0.85µl/min. The results of this investigation are shown in Fig. 3, from panel e to h.

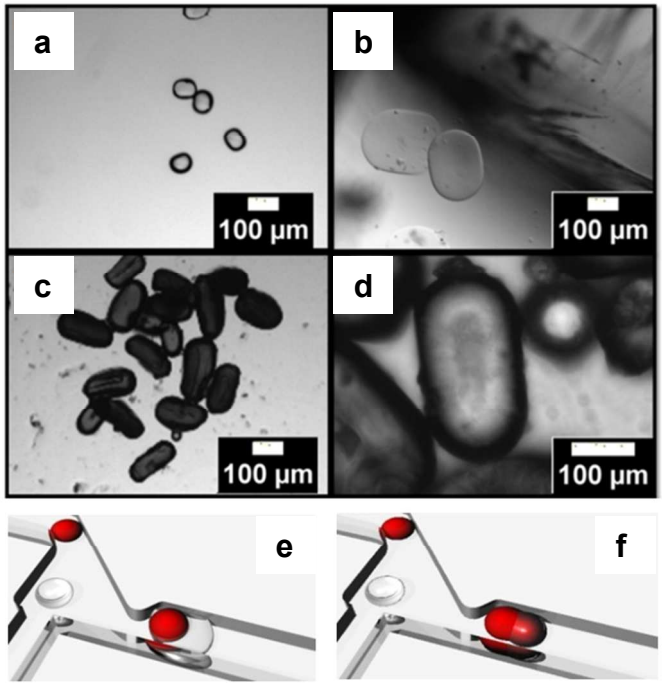

Fig. 5. Microgels dried. Microgels low aspect ratio with formaldehyde: a) Low Magnification b) High Magnification. Microgels high aspect ratio with glutaraldehyde: c) Low Magnification d) High Magnification. e) Cartoon of the mechanism displaying drop-in-drop coalescence (formaldehyde). f) Cartoon of the mechanism of coalescence with glutaraldehyde.

In the experiments carried out with high viscous streams, it was observed that the fusion of droplets took place within the shuffling element (Fig.3e-3f). In contrast to water based system, the curvature radius could not be identified in both the analysed timeframes. As, while the droplet B is forming, this already included the droplet A.
The results of the numerical investigations are displayed in panels reported in Fig. 3g and Fig. 3h. They show that once the droplets crossed the geometrical neck they were already fused. Indeed, it was not possible to distinguish the nuclei of the two droplets but one unique nucleus was observed.
Coalescence usually requires synchronisation and identical phase of the droplets. In order to achieve those requirements for droplet formation and coalescence, some external influence or complex microfluidic designs are required. The challenge is to simplify the use of droplet generator, coalescence and unit operations.[5]To date, a better understanding of the mechanism of coalescence in microfluidics could enhance the knowledge of hydrodynamics and simultaneously enhance the use of microdroplets in many standard processes.

For studying the behaviour of the droplets during the coalescence, as mentioned above, previous works refer to

viscous and inertial effects inside the droplets. In general observation of coalescence, Paulsen et al. described a mechanism of inertial or viscous coalescence related to the fluid dynamics of the droplets. The Reynolds number of coalescence is a function of the curvature radius of neck of coalescence (which in turn is a function of the time) and viscosity as well as density of the droplets.[5] In general, viscous and inertial coalescence were identified by Reynolds number, function of the curvature radius of the neck of coalescence. It was reported that for purely viscous coalescence the radius R of the liquid neck raised linearly with time t, as opposed to inertial coalescence where R increased with $t^{½}$. [8]

Here, our interest was focused on the behaviour of the fluid in the microchannels, as the droplets are affected by the fluid dynamics that there is developed.

Due to the overlapping with experimental data, the numerical results were used to estimate Reynolds number ($Re=dv\rho/\mu$where d is the characteristic size of the channel, v the velocity of the droplets, ρ and μ respectively the density and the viscosity of the streams). Reynolds number was recorded at five different positions along the channel, as displayed in Fig.4.

At $Q_B=Q_B*$ for the water-oil-water system, Reynolds number was Re>1, and it became Re=2 at the site of coalescence. By increasing the viscosity of the system (water-oil-protein system), Reynolds number became Re=0.5 along the channel and it reached the critical value of Re=1 at the point of coalescence.

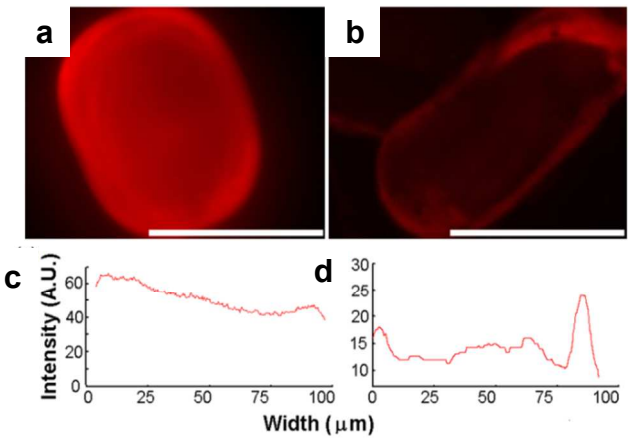

Fig.7. Absorption of rhodamine. a) Microgels stabilized by formaldehyde. b) Microgels stabilised by glutaraldehyde. Intensity of fluorescence along the width of the microgels. The scale bar is 100μm. c) Microgels stabilised by formaldehyde. d) Microgels stabilised by glutaraldehyde.

With the analogy at Paulsen theory, where the Reynolds number was expressed as function of the curvature radius, it was observed that at high viscosity, the radius of curvature increased rapidly and the mechanism of coalescence took place between the shuffling element and the geometrical neck.

In opposite, for the system water-oil-water, the radius increased slowly and the coalescence took place once the droplets crossed the shuffling element along the linear channel.

The Reynolds number of the channel was Re<1 for the high viscous system (viscous) and it was Re>1 for the water based system (inertial).

Inside the droplets, the Reynolds number can be achieved at the position x_5 for both the conditions under considerations.

In particular, it $Re_{x5}=2$ for water based experiment, and $Re_{x5}=1$ for protein solutions.

In summary, the design of the microfluidic system allowed for fusion of the droplets even though the intrinsic properties of the fluid was changed (i.e. viscosity) displaying that the system was extremely flexible. Indeed, the system responded to the change by enabling two different mechanisms of coalescence that were comparable to the viscous and inertial mechanisms of coalescence recorded in natural phenomena.

In general, the discrimination could be done by analysing Reynolds number of the droplet based on the curvature radius. Indeed, we analysed the Reynolds number of the flow in the microfluidic channel. Reynolds was Re<1 for high viscosity system and Re>1 for inertial regime. In conclusion, Reynolds number of the microfluidic channel followed the trend of the droplet fusion which simplified the analysis of the system.

Moreover, the control of coalescence via the viscous and inertial mechanisms may open up a wider range of future applications for the microfluidic channel.

3.3. Coalescence for stabilisation of microgels

The extensive characterisation of the microfluidic device clearly showed that the design was versatile to perform coalescence of droplets and that the mode of coalescence depended on fluid properties such as viscosity. The possibility to coalesce droplets with different properties and composition made the device intriguingly interesting for the fabrication of micro-particles with tailored properties and geometries. In particular, here, the fabrication of non spherical particles from proteins such as gelatin was the target application. Many advantages were directly related to the formation and stabilisation of microgels. Firstly, the microfluidic channel resembled the mould for the preparation of the microgels, so that several geometric shapes, from spheres to rods, can in theory be fabricated, thereby reproducing the dimension (width) of the channel, and length (controlled by the flow rates). [23-25]

Furthermore, small volumes of samples could be used to prepare the microgels in a high-throughput process. To produce the microgels, the stream A consisted of a solution of protein (15 wt:v%, gelatin), the flow B consisted of aldehyde solution and the flow C consisted of fluorinated oil. The reaction stabilised the gelatin, by oxidation of the carboxylic groups i.e. by cross-linking.

Formaldehyde and glutaraldehyde were used to perform the crosslink reaction. As mentioned earlier, coalescence occurs inside the shuffling element at Re<1 for high viscosity solutions. Moreover, when using the two cross-linkers mentioned above, analysing the behaviour of the systems, differences between the two modes of coalescence were still

identified, displaying once more that this mechanism was indeed a function of the properties of the fluids.

Microparticles stabilised by formaldehyde were shown in Fig. 5a and Fig. 5b (low and high magnification respectively). They displayed an aspect ratio (length-to-width) scantly higher than 1.3.

Microparticles stabilised by the glutaraldehyde displayed higher aspect ratio (close to 3.5) (Fig. 5c and Fig. 5d low and high magnification).

To explain the different aspect ratios, the properties of the two aldehydes were considered.

Glutaraldehyde and formaldehyde displayed different strengths for protein crosslinking, to date the standard protocol requires smaller concentration of first than the latter.

For the microfluidic experiment, the concentration of formaldehyde was 10% and the concentration of glutaraldehyde was 1%. In particular, the properties (viscosity and wettability) of the formaldehyde solution was much different compared to water (10% Formaldehyde: viscosity 2.045×10^{-3} Pa s,[26] versus 8.9×10^{-4} Pa s viscosity of water), the properties of the glutaraldehyde solution were closer to water.

As function of the pressure tension (deriving from the moles of solute in water), the chemical potential changes and the mixing is directly affected by those differences. To date, due to the different properties of the fluid, two different sub-conditions for coalescence were identified. Formaldehyde solution generated *drop-in-drop-coalescence* that resembled compartmentalisation of gelatin inside the microdroplet of formaldehyde (Fig. 5e). In formaldehyde, the particles of gelatin were stabilised following a mechanism already observed in our previous investigation carried out with ethanol and gelatin.[27] As consequence of compartmentalisation, low aspect ratio particles were fabricated (Fig. 5a).

The strength of gluteraldehyde cross-linking was very high and only a low concentration was required to fix the gelatin. The mechanisms of mixing is shown in Fig. 5f displaying that gelatin and glutaraldehyde mix together indeed the gelatin spread inside the droplet of glutaraldehyde. The particles had high aspect ratio (Fig. 5c).

An advantage of stabilisation by glutaraldehyde was the possibility to fabricate the microparticles in-flow which might make it possible to cast the particles during the reaction and obtained considerably high aspect ratio particles (**see Fig. 4S in Supporting Information).**

The different methods of stabilisation reported above influenced the behaviour of the particles.

Both the families of particles were incubated with a solution containing rhodamine in water and analysed to track the fluorescent signal across the section. The results of the investigation are reported in Fig. 6a and Fig. 6b.

Thetwo families of microparticles displayed different profiles of fluorescence. Formaldehyde stabilised particles displayed flat and high fluorescence profile (Fig. 6c); in contrast, glutaraldehyde stabilised particles displayed peaks of fluorescence at the surface but low intensity inside the core of the droplets (Fig. 6d).

The rhodamine was able to penetrate through the microstructure of the particle stabilised by formaldehyde, whilst it was not able to penetrate as far as to the core of the structure. The different microstructures influenced the mechanism of degradation of the particles. The rhodamine molecules were selected for the absorption as they can simulate the behaviour of many drugs and molecule compounds used for therapies. As such this enabled to predict model of absorption and delivery. To further test the different properties of the particles, they were incubated with trypsin. Trypsin is normally used to digest proteins.

During the time of digestion, the microparticles were observed at the microscope. Once elapsed the first hour, the particles stabilised by formaldehyde were digested by the trypsin and they were dissolved in the solution. The mechanism of degradation of the particles with glutaraldehyde displayed slower mechanism of digestion (Fig. 7). The panels a, b and c in Fig. 7 display three different timeframes of the particle degradation.

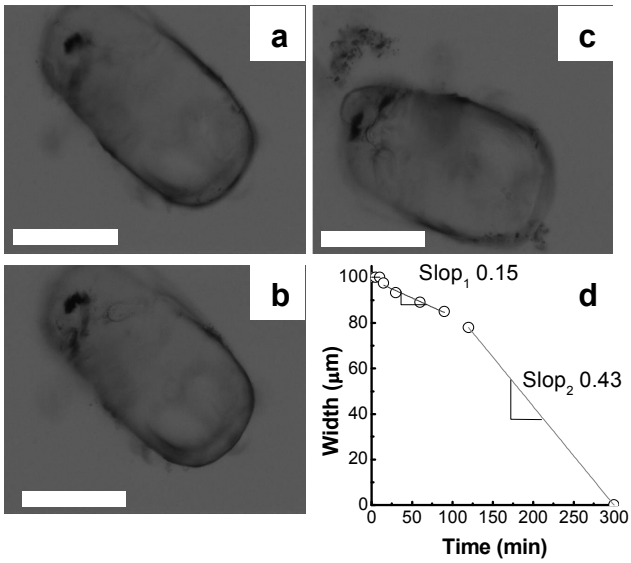

Fig.7. Pictures of the microgel stabilized by glutaraldehyde during the degradation: a) 45 min; b) 100 min; c) 120 min. d) Velocity of degradation of the stabilized particles in microfluidic channels. The scale bar is 100µm.

During the first instant (15 min) of the reaction, the activity of the trypsin was low and negligible. The velocity of degradation increased during the first hour of experiment. In the subsequent hours, the velocity further increased (three folds). The complete digestion of the particles occurred in 5 hours. To date we studied the kinetic of degradation of the particles. The velocity of degradation (v_{dg}) was the variation of the width (W) (observed by high magnification microscope) according to the time. The expression of the velocity of degradation is $v_{dg}=dW/dt$.

The differences of v_{dg} during the experiment until the complete digestion of the particles were due to the barrier that the trypsin encountered to penetrate the shell of the crosslinked gelatin.

The velocity of degradation increased and after an initial slow mechanism, and the trypsin quickly digested the core of the

microgels. The difference between the two velocities of degradation was also symptomatic of two different microstructures. A ´higher crosslinked´ external shell encapsulates a ´softer core´ or uniform networking were obtained with formaldehyde and glutaraldehyde respectively.

4. Conclusions

Coalescence of droplets performed in microfluidic channels was performed in a system independently on phase and synchronisation of the droplets. Indeed, the most important parameter is related to the composition of the droplets.
Numerical and experimental investigations were carried out to characterise the mechanisms of coalescence for low and high viscous samples. Mimicking the phenomena occurring in Nature, inertial and viscous coalescence was observed owing to the intrinsic properties of the perfused fluid.
The possibility to coalesce droplets with different properties and composition made this research interesting for the fabrication of micro-particles with tailored properties and geometries.
In particular, the investigation has been focused on the fabrication of nonspherical particles from proteins such as gelatin. Many advantages were directly related to the formation and stabilisation of microgels. Firstly, the microfluidic channel resembled the mould for the preparation of the microgels, so that several geometric shapes, from spheres to rods, can in theory be fabricated, thereby reproducing the dimension (width) of the channel, and length (controlled by the flow rates).
The microfluidic system was used to cast microgels based on proteins stabilised by aldehyde compounds. The microgels displayed different aspect ratio and properties depending on the stabiliser. The formaldehyde enabled faster stabilisation creating a gradient of crosslink from outside to inside; the glutaraldehyde enabled high extent of crosslink across the whole geometry.
Then, as the microgels have been produced by native proteins, the biodegradability of the particles has been also characterised suggesting the microgels for biological applications.
The tunability of the micromechanical properties of the microgels as well as the ease of functionalisation indicates clearly that our method has a high potential in several biomedical research fields. The proposed application of the microfluidic device requires dealing with samples with specific chemical-physics behaviour. To date, a better understanding of the mechanisms of coalescence in microfluidics could enhance the knowledge of hydrodynamics and simultaneously enhance the use of microdroplets in many standard processes.

Acknowledgements

The author wants to thank Dr.P. Löthman for proofreading and Dr. A. Pepe for the contribution during her Master project.

Notes and references

[a]University of Naples "Federico II", Piazzale Tecchio, 80- 80125 Napoli-Italy.Email giuseppina.simone@unina.it

Electronic Supplementary Information (ESI) available: details of any supplementary information available should be included here. See DOI: 10.1039/b000000x/

1. F. Blanchette, T. P. Bigioni, *Nat Phys,* 2006, **2,** 254-257.
2. S. B. Lang, C. R. Wilke, *Industrial & Engineering Chemistry Fundamentals*, 1971, **10**, 341.
3. J. D. Paulsen, R. Carmigniani, A. Kannan, J. C. Burton, S. R. Nagel, *Nat Commun*, 2014, **5**, 3182.
4. A. R. Thiam, R. V. Farese Jr, T. C. Walther, The biophysics and cell biology of lipid droplets, *Nat Rev Mol Cell Biol*, 2013, **14**, 775.
5. J. D. Paulsen, J. C. Burton, S. R. Nagel, Viscous to Inertial Crossover in Liquid Drop Coalescence, *Physical Review Letters,* 2011, **106**, 114501.
6. J. D. Paulsen, J. C. Burton, S. R. Nagel, S. Appathurai, M. T. Harris, O. A. Basaran, *Proceedings of the National Academy of Sciences*, 2012, **109**, 6857.
7. S. A. K. Jeelani, R. Hosig, E. J. Windhab, *AIChE Journal,* 2005, **51**, 149.
8. J. D. Paulsen, *Physical Review* 2013, **E88** , 063010.
9. N. Bremond, J. Bibette, *Soft Matter,* 2012, **8**, 10549.
10. L. Mazutis, A. D. Griffiths, *Lab on a chip*, 2012, **12**, 1800.
11. V. Chokkalingam, B. Weidenhof, M. Kramer, W. F. Maier, S. Herminghaus, R. Seemann, *Lab on a chip* ,2010, **10**, 1700.
12. K. Maeda, H. Onoe, M. Takinoue, S. Takeuchi, *Advanced materials*, 2012, **24**, 1340.
13. A. R. Studart, H. C. Shum, D. A. Weitz, *The Journal of Physical Chemistry B*, 2009, **113**, 3914.
14. N. Yi, B. Huang, L. Dong, X. Quan, F. Hong, P. Tao, C. Song, W. Shang, T. Deng, *Sci. Rep*. 2014, **4** , 4303.
15. H. Gu, M. H. G. Duits, F. Mugele, *International Journal of Molecular Sciences*, 2011, **12**, 2572.
16. G. Simone, G. Perozziello, *Journal of Nanoscience and Nanotechnology*, 2011, **11**, 2057.
17. G. Simone, G. Perozziello, G. Sardella, I. Disegna, S. Tori, N. Manaresi, G. Medoro, *Microsyst Technol,* 2010, **16**, 1269.
18. G. Simone, Protocols and pipelines to fabricate microgels in microfluidics, LAPLAMBERT Academic Publishing, October 12, 2013, ISBN-10: 3659475939.
19. G. Simone, P. A. Netti, *Microelectronic Engineering*, 2013, **111**, 339.
20. M. Denn Process Fluid Mechanics. New Jersey: Prentice-Hall International Series in the Physical and Chemical Engineering Sciences, 1980.
21. Lord Byron Bird Transport Phenomena, Revised 2nd Edition by R. Byron Bird, Warren E. Stewart and Edwin N. Lightfoot, 2006.
22. D.R. LIDE, ed. 2001. Handbook of Chemistry and Physics, CRC Press, Boca Raton/New York/London/Tokyo.
23. J. T. Wang, J. Wang, J. J. Han, *Small*, 2011, **7**, 1728.
24. Y. Li, G. Huang, X. Zhang, B. Li, Y. Chen, T. Lu, T. J. Lu, F. Xu, *Advanced Functional Materials*, 2013, **23**, 660.
25. J.-C. Pothier, L. J. Lewis, *Physical Review B*, 2012, **85**, 115447.
26. J. G. M. Winkelman, A. A. C. M. Beenackers, *Industrial & Engineering Chemistry Research*, 2000, **39**, 557.

27. G. Simone, et al. 16th International Conference on Miniaturized Systems for Chemistry and Life Sciences October 28 - November 1, 2012, Okinawa, Japan.

